Identification of boundary heat flux assuring the destruction of target region of biological tissue – application of the generalized dual-phase lag model and gradient method

Lukasz Turchan, Ewa Majchrzak

Institute of Computational Mechanics and Engineering
Silesian University of Technology
Konarskiego 18A, 44-100 Gliwice, Poland
e-mail: lukasz.turchan@polsl.pl

In this paper, an axially symmetrical biological tissue domain subjected to an external heat source is analyzed. The thermal processes occurring in the domain considered are described using the generalized dual-phase lag model supplemented by the Neumann boundary conditions and the appropriate initial conditions. The problem of tissue heating is solved using the implicit scheme of the finite difference method. The obtained solution allows one to determine the local and temporary values of the Arrhenius integral. Next, the inverse problem related to the identification of the boundary heat flux assuring the postulated destruction of the tissue target region is considered. The problem is solved using the gradient method. In the final part of the paper, the results of computations and the conclusions are presented.

Keywords: bioheat transfer, generalized dual-phase lag model, Arrhenius integral, inverse problem, finite difference method, gradient method.

1. INTRODUCTION

One of the important issues related to the impact of high temperatures on biological tissue is the estimation of its destruction. From the mathematical point of view, to achieve this goal, the Arrhenius integral [1–3] can be used. To calculate the Arrhenius integral, the temperature distribution in the domain of biological tissue should be known. Numerous models describing the bioheat transfer can be found in literature, e.g., Pennes equation [4–9], Cattaneo-Vernotte equation [10–12], dual-phase lag model [13–18] or generalized dual-phase lag model [19–22]. In this paper, the generalized dual-phase lag model is used. This model is based on the theory of porous media [23], and then the biological tissue is divided into two regions: the vascular region (blood vessel) and the extravascular region (tissue) [24, 25]. The mathematical model consists of two coupled equations describing the tissue and blood temperature, respectively. In the generalized dual-phase lag equation (GDPLE) concerning the tissue sub-domain, the phase lag times appear, namely the relaxation time and thermalization time. The phase lag times are expressed in terms of the blood and tissue properties, the interphase convective heat transfer coefficient and the blood perfusion rate. The equations are supplemented by appropriate boundary and initial conditions. Formulated in this way problem can be solved using the numerical method. The implicit scheme of finite difference method is applied here. Knowing the spatial-temporal distribution of the tissue temperature, the Arrhenius integral can be calculated.

In the inverse problem considered here, based on the knowledge of the Arrhenius integral at the set of measuring points of the domain, the parameters of the Neumann boundary condition are identified. To determine these parameters, the gradient method [26–28] is used. Sensitivity

coefficients occurring in the gradient method are calculated using the direct approach of sensitivity analysis [29–31].

It should be noted that a similar problem is presented in [32], but here the two-temperature generalized dual-phase lag model is used, which better reflects thermal processes occurring in heated tissues.

The proposed procedure can be helpful in planning artificial hyperthermia treatment because it allows to predict the amount of necessary heat delivered to the tissue that ensures the destruction of the target region.

2. Direct problem

An axially symmetrical domain of biological tissue exposed to an external heat source is considered. Thermal processes can be described by the generalized dual-phase lag model [21, 22, 25]:

$$(r,z) \in \Omega: \quad C\left(\frac{\partial T}{\partial t} + \tau_q \frac{\partial^2 T}{\partial t^2}\right) = \Lambda\left[\nabla^2 T + \tau_T \frac{\partial}{\partial t}\left(\nabla^2 T\right)\right]$$

$$+ G(T_b - T) + \varepsilon Q_b + (1 - \varepsilon) Q + \frac{\tau_q C}{(1 - \varepsilon)\rho c}\left[\varepsilon \frac{\partial Q_b}{\partial t} + (1 - \varepsilon)\frac{\partial Q}{\partial t}\right] \quad (1)$$

and

$$T_b = T - \frac{\varepsilon \rho_b c_b}{G}\frac{\partial T_b}{\partial t}, \tag{2}$$

where $T = T(r, z, t)$, $T_b = T_b(r, z, t)$ are the tissue and blood temperatures, respectively, r, z are the spatial coordinates, t is the time, ε denotes the porosity (the ratio of blood volume to the total volume), ρ, ρ_b are the densities of tissue and blood, respectively, c, c_b are the specific heats, Q, Q_b are the metabolic heat sources, while

$$\Lambda = (1 - \varepsilon)\lambda + \varepsilon \lambda_b \tag{3}$$

and

$$C = (1 - \varepsilon)\rho c + \varepsilon \rho_b c_b \tag{4}$$

are the effective thermal conductivity (λ, λ_b are the thermal conductivities of tissue and blood) and effective heat capacity, respectively.

The coupling factor G is expressed as [19, 21]

$$G = A\alpha + w c_b, \tag{5}$$

where A is the volumetric heat transfer area between tissue and blood, α is the heat transfer coefficient, and w is the blood perfusion rate.

In Eq. (1) τ_q is the relaxation time and τ_T is the thermalization time. These phase lags are defined as follows [19, 21]:

$$\tau_q = \frac{\varepsilon (1 - \varepsilon)\rho c \rho_b c_b}{G C} \tag{6}$$

and

$$\tau_T = \frac{\varepsilon (1 - \varepsilon)\rho_b c_b \lambda}{G \Lambda}. \tag{7}$$

In the dual-phase lag model, the Neumann condition takes a form [17, 18]

$$(r,z) \in \Gamma: \quad -\lambda \left[\mathbf{n} \cdot \nabla T\left(r,z,t\right) + \tau_T \frac{\partial \left[\mathbf{n} \cdot \nabla T\left(r,z,,t\right)\right]}{\partial t} \right] = q_b\left(r,z,t\right) + \tau_q \frac{\partial q_b\left(r,z,t\right)}{\partial t}, \tag{8}$$

where $\mathbf{n}$ is the normal outward vector, $\mathbf{n} \cdot \nabla T\left(r,z,t\right)$ is the derivative of temperature in the normal direction, while $q_b(r,z,t)$ is known boundary heat flux.

On the upper surface of the domain, the following boundary heat flux is assumed:

$$q_b(r,0,t) = \begin{cases} q_0 \dfrac{t}{t_e}\left(1 - \dfrac{t}{t_e}\right)\exp\left(-\dfrac{r^2}{r_D^2}\right), & t \le t_e, \\ 0, & t > 0, \end{cases} \tag{9}$$

where q_0 is the constant value and t_e is the exposure time, while $r_D \le R$ where R is the radius of the cylinder. On the remaining boundaries, the no-heat flux conditions can be accepted ($q_b(r,z,t) = 0$). The initial conditions are also known:

$$t = 0: \quad T\left(r,z,0\right) = T_0, \qquad \left.\frac{\partial T\left(r,z,t\right)}{\partial t}\right|_{t=0} = u(r,z), \qquad T_b\left(r,z,0\right) = T_0, \tag{10}$$

where T_0 is the constant initial temperature and $u(r,z)$ is the initial heating rate.

The thermal damage parameter can be evaluated according to the Arrhenius integral [1–3, 33]:

$$A\left(r,z,t^f\right) = P \int_0^{t^f} \exp\left(-\frac{E}{R_g T(r,z,t)}\right) \mathrm{d}t, \tag{11}$$

where P is the pre-exponential factor, E is the activation energy, R_g is the universal gas constant, $T(r,z,t)$ is the tissue temperature, and $[0,t^f]$ is the time interval under consideration.

A value of damage integral $A(r,z,t^f) = 1$ corresponds to a 63% probability of cell death at a specific point, while $A(r,z,t^f) = 4.6$ corresponds to 99% probability of cell death at this point.

3. SENSITIVITY ANALYSIS

The purpose of the research is to estimate the boundary heat flux (9), more specifically, the values q_0 and t_e, which ensure the destruction of the target region of biological tissue. Thus, at first, the sensitivity analysis [28–31] of tissue temperature and blood temperature with respect to q_0 and t_e will be carried out.

The governing equations are differentiated with respect to the parameter p_s, $s = 1,2$, where $p_1 = q_0$, $p_2 = t_e$. The differentiation of Eqs (1) and (2) gives

$$(r,z) \in \Omega: \quad C\left(\frac{\partial U_s}{\partial t} + \tau_q \frac{\partial^2 U_s}{\partial t^2}\right) = \Lambda\left[\nabla^2 U_s + \tau_T \frac{\partial}{\partial t}\left(\nabla^2 U_s\right)\right] - GU_s, \tag{12}$$

and

$$U_{bs} = U_s - \frac{\varepsilon \rho_b c_b}{G} \frac{\partial U_{bs}}{\partial t}, \tag{13}$$

where $U_s = \partial T / \partial p_s$, $U_{bs} = \partial T_b / \partial p_s$ are sensitivity functions, $s = 1,2$. It should be noted that in Eq. (1) the constant values of Q and Q_b are assumed.

Differentiation of boundary condition (8) gives

$$-\lambda\left\{\mathbf{n} \cdot \nabla U_s(r,z,t) + \tau_T \frac{\partial}{\partial t}\left[\mathbf{n} \cdot U_s(r,z,t)\right]\right\} = \frac{\partial q_b\left(r,z,t\right)}{\partial p_s} + \tau_q \frac{\partial}{\partial t}\left[\frac{\partial q_b\left(r,z,t\right)}{\partial p_s}\right], \tag{14}$$

where ($p_1 = q_0$)

$$\frac{\partial q_b(r,0,t)}{\partial q_0} = \begin{cases} \dfrac{t}{t_e}\left(1 - \dfrac{t}{t_e}\right)\exp\left(-\dfrac{r^2}{r_D^2}\right), & t \le t_e, \\ 0, & t > 0, \end{cases} \tag{15}$$

and ($p_2 = t_e$)

$$\frac{\partial q_b(r,0,t)}{\partial t_e} = \begin{cases} q_0\dfrac{t}{t_e^2}\left(2\dfrac{t}{t_e} - 1\right)\exp\left(-\dfrac{r^2}{r_D^2}\right), & t \le t_e, \\ 0, & t > 0. \end{cases} \tag{16}$$

The initial conditions (10) are also differentiated

$$t = 0: \quad U_s(r,z,0) = 0, \qquad \left.\frac{\partial U_s(r,z,t)}{\partial t}\right|_{t=0} = 0, \qquad U_{bs}(r,z,0) = 0. \tag{17}$$

Finally, the Arrhenius integral (11) is differentiated with respect to the parameter p_s

$$R_s(r,z,t^f) = P\int_0^{t^f} \frac{E}{R_g T^2(r,z,t)}\exp\left(-\frac{E}{R_g T(r,z,t)}\right)U_s(r,z,t)\mathrm{d}t. \tag{18}$$

To solve the direct problem and additional problems related to the sensitivity analysis, the implicit scheme of the finite difference method is used.

4. FINITE DIFFERENCE METHOD

A structure of Eqs (1) and (12) is similar, they can be therefore written in the form:

$$C\left(\frac{\partial Z_s}{\partial t} + \tau_q\frac{\partial^2 Z_s}{\partial t^2}\right) = \Lambda\left[\nabla^2 Z_s + \tau_T\frac{\partial}{\partial t}\left(\nabla^2 Z_s\right)\right] - GZ_s + GT_b + \varepsilon Q_b + (1-\varepsilon)Q, \tag{19}$$

where $Z_0(r,z,t) = T(r,z,t)$, $Z_s(r,z,t) = U_s(r,z,t)$, $s = 1,2$ and

$$W_s = \begin{cases} GT_b + \varepsilon Q_b + (1-\varepsilon)Q, & s = 0, \\ 0, & s = 1,2. \end{cases} \tag{20}$$

Equations (2) and (13) can be expressed as follows:

$$Z_{bs} = Z_s - \frac{\varepsilon\rho_b c_b}{G}\frac{\partial Z_{bs}}{\partial t}, \tag{21}$$

where $Z_{b0}(r,z,t) = T_b(r,z,t)$, $Z_{bs}(r,z,t) = U_{bs}(r,z,t)$, $s = 1,2$.

The boundary conditions (8) and (14) take a form

$$(r,z) \in \Gamma: \quad -\Lambda\left\{\mathbf{n}\cdot\nabla Z_s(r,z,t) + \tau_T\frac{\partial}{\partial t}\left[\mathbf{n}\cdot Z_s(r,z,t)\right]\right\} = V_s(r,z,t), \tag{22}$$

where

$$V_s(r,z,t) = \begin{cases} q_b(r,z,t) + \tau_q\dfrac{\partial q_b(r,z,t)}{\partial t}, & s = 0, \\ \dfrac{\partial q_b(r,z,t)}{\partial p_s} + \tau_q\dfrac{\partial}{\partial t}\left[\dfrac{\partial q_b(r,z,t)}{\partial p_s}\right], & s = 1,2. \end{cases} \tag{23}$$

Equations (19)–(23) are supplemented by the initial conditions (10) and (17).

The basic problem and additional ones connected with the sensitivity functions are solved using the implicit scheme of finite difference method.

The following approximation of Eq. (19) is proposed:

$$C\left(\frac{Z_{i,j}^{f} - Z_{i,j}^{f-1}}{\Delta t} + \tau_q \frac{Z_{i,j}^{f} - 2Z_{i,j}^{f-1} + Z_{i,j}^{f-2}}{(\Delta t)^2}\right) = \Lambda\left(\nabla^2 Z_{i,j}^{f} + \tau_T \frac{\nabla^2 Z_{i,j}^{f} - \nabla^2 Z_{i,j}^{f-1}}{\Delta t}\right) - GZ_{i,j}^{f} + W_s, \quad (24)$$

where

$$\nabla^2 Z_{i,j}^{f} = \frac{Z_{i,j-1}^{f} - 2Z_{i,j}^{f} + Z_{i,j+1}^{f}}{h^2} + \frac{1}{r_{i,j}}\frac{Z_{i,j+1}^{f} - Z_{i,j-1}^{f}}{2h} + \frac{Z_{i-1,j}^{f} - 2Z_{i,j}^{f} + Z_{i+1,j}^{f}}{h^2},$$

$$\nabla^2 Z_{i,j}^{f-1} = \frac{Z_{i,j-1}^{f-1} - 2Z_{i,j}^{f-1} + Z_{i,j+1}^{f-1}}{h^2} + \frac{1}{r_{i,j}}\frac{Z_{i,j+1}^{f-1} - Z_{i,j-1}^{f-1}}{2h} + \frac{Z_{i-1,j}^{f-1} - 2Z_{i,j}^{f-1} + Z_{i+1,j}^{f-1}}{h^2}, \quad (25)$$

while Δt is the time step, h is the grid step. In the above equations, index s is omitted for simplification.

After mathematical manipulations we obtain

$$Z_{i,j}^{f} = \frac{\Lambda\Delta t(\Delta t + \tau_T)}{D}\left(Z_{i-1,j}^{f} + Z_{i+1,j}^{f} + \frac{2r_{i,j} - h}{2r_{i,j}}Z_{i,j-1}^{f} + \frac{2r_{i,j} + h}{2r_{i,j}}Z_{i,j+1}^{f}\right)$$

$$- \frac{\Lambda\Delta t\tau_T}{D}\left(Z_{i-1,j}^{f-1} + Z_{i+1,j}^{f-1} + \frac{2r_{i,j} - h}{2r_{i,j}}Z_{i,j-1}^{f-1} + \frac{2r_{i,j} + h}{2r_{i,j}}Z_{i,j+1}^{f-1}\right)$$

$$+ \frac{Ch^2(\Delta t + 2\tau_q) + 4\Lambda\Delta t\tau_T}{D}Z_{i,j}^{f-1} - \frac{Ch^2\tau_q}{D}Z_{i,j}^{f-2} + \frac{h^2(\Delta t)^2}{D}W_s, \quad (26)$$

where

$$D = h^2\left[C(\Delta t + \tau_q) + G(\Delta t)^2\right] + 4\Lambda\Delta t(\Delta t + \tau_T). \quad (27)$$

The approximation of the boundary conditions (22) is as follows:

$$-\Lambda\left\{\mathbf{n}\cdot\nabla Z_s(r,z,t^f) + \frac{\tau_T}{\Delta t}\left[\mathbf{n}\cdot Z_s(r,z,t^f) - \mathbf{n}\cdot Z_s(r,z,t^{f-1})\right]\right\} = V_s(r,z,t^f). \quad (28)$$

Thus, we obtain the formulas:

- for $j = 1, 2, ..., n-1$

$$Z_{0,j}^{f} = Z_{1,j}^{f} - \frac{\tau_T}{\Delta t + \tau_T}\left(Z_{0,j}^{f-1} - Z_{1,j}^{f-1}\right) + \frac{h\Delta t}{\Lambda(\Delta t + \tau_T)}V_{0,j}^{f}, \quad (29)$$

$$Z_{n,j}^{f} = Z_{n-1,j}^{f} + \frac{\tau_T}{\Delta t + \tau_T}\left(Z_{n,j}^{f-1} - Z_{n-1,j}^{f-1}\right) - \frac{h\Delta t}{\Lambda(\Delta t + \tau_T)}V_{n,j}^{f}, \quad (30)$$

- for $i = 1, 2, ..., n-1$

$$Z_{i,0}^{f} = Z_{i,1}^{f} - \frac{\tau_T}{\Delta t + \tau_T}\left(Z_{i,1}^{f-1} - Z_{i,0}^{f-1}\right) - \frac{r_{i,0}h\Delta t}{\Lambda(\Delta t + \tau_T)}V_{i,0}^{f}, \quad (31)$$

$$Z_{i,n}^{f} = Z_{i,n-1}^{f} + \frac{\tau_T}{\Delta t + \tau_T}\left(Z_{i,n}^{f-1} - Z_{i,n-1}^{f-1}\right) - \frac{r_{i,n}h\Delta t}{\Lambda(\Delta t + \tau_T)}V_{i,n}^{f}. \quad (32)$$

Finally, Eq. (21) is approximated:

$$Z_{bi,j}^f = Z_{i,j}^f - \frac{\varepsilon \rho_b c_b}{G} \frac{Z_{bi,j}^f - Z_{bi,j}^{f-1}}{\Delta t}, \tag{33}$$

and then

$$Z_{bi,j}^f = \frac{G \Delta t}{G \Delta t + \varepsilon \rho_b c_b} Z_{i,j}^f + \frac{\varepsilon \rho_b c_b}{G \Delta t + \varepsilon \rho_b c_b} Z_{bi,j}^{f-1}. \tag{34}$$

The system of Eqs (26) and (34) supplemented by boundary conditions (29)–(32) and initial conditions (10) and (17) is solved using the iterative method.

5. INVERSE PROBLEM

As mentioned earlier, the inverse problem formulated here concerns the estimation of the parameters q_0 and t_e occurring in the boundary heat flux (9). Thus, the following criterion is formulated:

$$S(q_0, t_e) = \sum_{f=1}^{F} \sum_{i=1}^{M} \left[A(r_i, z_i, t^f, q_0, t_e) - A_m(r_i, z_i, t^f) \right]^2, \tag{35}$$

where $A_m(r_i, z_i, t^f)$ is the 'measured' Arrhenius integral. $A(r_i, z_i, t^f, q_0, t_e)$ is the calculated Arrhenius integral obtained from the direct problem solution with the current estimation of the unknown parameters q_0 and t_e, while M is the number of points and F is the number of time steps.

In the case of typical gradient method application [26–28] the criterion (35) is differentiated with respect to the unknown parameters q_0, t_e, and next, the necessary condition of the optimum is used. Thus, one obtains the following system of equations (c.f. formula (18))

$$\frac{\partial S(q_0, t_e)}{\partial q_0} = 2 \sum_{f=1}^{F} \sum_{i=1}^{M} \left(A_i^f - A_{m,i}^f \right) R_{1,i}^f = 0,$$

$$\frac{\partial S(q_0, t_e)}{\partial t_e} = 2 \sum_{f=1}^{F} \sum_{i=1}^{M} \left(A_i^f - A_{m,i}^f \right) R_{2,i}^f = 0, \tag{36}$$

where $A_i^f = A\left(r_i, z_i, t^f, q_0, t_e\right)$, $A_{m,i}^f = A\left(r_i, z_i, t^f\right)$.

The function A_i^f is expanded into a Taylor series for the known values of q_0^k and t_e^k, this means

$$A_i^f = \left(A_i^f \right)^k + \left(R_{1,i}^f \right)^k \left(q_0^{k+1} - q_0^k \right) + \left(R_{2,i}^f \right)^k \left(t_e^{k+1} - t_e^k \right), \tag{37}$$

where k is the number of iteration, q_0^k and t_e^k for $k = 0$ are the arbitrary assumed values of q_0 and t_e, while for $k > 0$ q_0^k and t_e^k result from the previous iteration.

Introducing formula (37) to Eq. (36) one obtains

$$\sum_{f=1}^{F} \sum_{i=1}^{M} \left[\left(A_i^f \right)^k + \left(R_{1,i}^f \right)^k \left(q_0^{k+1} - q_0^k \right) + \left(R_{2,i}^f \right)^k \left(t_e^{k+1} - t_e^k \right) - A_{m,i}^f \right] \left(R_{1,i}^f \right)^k = 0,$$

$$\sum_{f=1}^{F} \sum_{i=1}^{M} \left[\left(A_i^f \right)^k + \left(R_{1,i}^f \right)^k \left(q_0^{k+1} - q_0^k \right) + \left(R_{2,i}^f \right)^k \left(t_e^{k+1} - t_e^k \right) - A_{m,i}^f \right] \left(R_{2,i}^f \right)^k = 0, \tag{38}$$

it means

$$\left(q_0^{k+1} - q_0^k\right) \sum_{f=1}^{F} \sum_{i=1}^{M} \left[\left(R_{1,i}^f\right)^k\right]^2 + \left(t_e^{k+1} - t_e^k\right) \sum_{f=1}^{F} \sum_{i=1}^{M} \left(R_{1,i}^f\right)^k \left(R_{2,i}^f\right)^k = \sum_{f=1}^{F} \sum_{i=1}^{M} \left[A_{m,i}^f - \left(A_i^f\right)^k\right] \left(R_{1,i}^f\right)^k,$$

$$\left(q_0^{k+1} - q_0^k\right) \sum_{f=1}^{F} \sum_{i=1}^{M} \left(R_{1,i}^f\right)^k \left(R_{2,i}^f\right)^k + \left(t_e^{k+1} - t_e^k\right) \sum_{f=1}^{F} \sum_{i=1}^{M} \left[\left(R_{2,i}^f\right)^k\right]^2 = \sum_{f=1}^{F} \sum_{i=1}^{M} \left[A_{m,i}^f - \left(A_i^f\right)^k\right] \left(R_{2,i}^f\right)^k,$$

(39)

or in the matrix form

$$\begin{bmatrix} \sum_{f=1}^{F} \sum_{i=1}^{M} \left[\left(R_{1,i}^f\right)^k\right]^2 & \sum_{f=1}^{F} \sum_{i=1}^{M} \left(R_{1,i}^f\right)^k \left(R_{2,i}^f\right)^k \\ \sum_{f=1}^{F} \sum_{i=1}^{M} \left(R_{1,i}^f\right)^k \left(R_{2,i}^f\right)^k & \sum_{f=1}^{F} \sum_{i=1}^{M} \left[\left(R_{2,i}^f\right)^k\right]^2 \end{bmatrix} \begin{bmatrix} \Delta q_0^k \\ \Delta t_e^k \end{bmatrix} = \begin{bmatrix} \sum_{f=1}^{F} \sum_{i=1}^{M} \left[A_{m,i}^f - \left(A_i^f\right)^k\right] \left(R_{1,i}^f\right)^k \\ \sum_{f=1}^{F} \sum_{i=1}^{M} \left[A_{m,i}^f - \left(A_i^f\right)^k\right] \left(R_{2,i}^f\right)^k \end{bmatrix}. \quad (40)$$

After solving the system of Eqs (40), the new values of identified parameters are determined using the formulas:

$$\begin{aligned} q_0^{k+1} &= q_0^k + \Delta q_0^k, \\ t_e^{k+1} &= t_e^k + \Delta t_e^k. \end{aligned} \quad (41)$$

The iterative process is continued until the assumed number K of iterations is achieved.

6. RESULTS OF COMPUTATIONS

An axially symmetrical domain of biological tissue is considered ($R = Z = 0.015$ m). The values of the parameters are collected in Table 1. It is assumed that in the Arrhenius integral (11) the activation energy is equal to $E = 6.67 \cdot 10^5$ J/mole, pre-exponential factor is equal to $P = 1.98 \cdot 10^{106}$ 1/s, and the universal gas constant: $R_g = 8.314472$ J/(mol K) [34, 35]. Three variants of porosity, as shown in Table 2, are considered.

Table 1. Values of parameters [23, 38].

Parameter	Tissue	Blood
Thermal conductivity [W/(m K)]	$\lambda_t = 0.5$	$\lambda_b = 0.5$
Specific heat [J/(kg K)]	$c_t = 4000$	$c_b = 3770$
Density [kg/m^3]	$\rho_t = 1000$	$\rho_b = 1060$
Metabolic heat source [W/m^3]	$Q_{mt} = 250$	$Q_{mb} = 250$
Initial temperature [°C]	$T_p = 37$	$T_p = 37$

Table 2. Variants of porosity [19, 22].

Variant	ε	G [W/(m^{3}K)]	τ_q [s]	τ_T [s]	w [kg/(m^{3}s)]
v$_1$	0.0041	34 785.174	0.46772	0.46771	1
v$_2$	0.0357	79 102.601	1.74116	1.74110	3
v$_3$	0.1637	96 479.910	5.67173	5.67085	5

At first, the direct problem is solved under the assumption that $q_0 = 15\,000$ W/m^2, $t_e = 200$ s, (c.f. Eq. (9)) and $r_D = R/4$. The spatial grid step is $h = 0.0003$ m and the time step $\Delta t = 0.1$ s.

In Fig. 1, the tissue temperature distribution after 120 s is shown, while Fig. 2 illustrates the tissue temperature history at two selected points from the considered domain. As it is visible,

the higher the porosity value, the lower the tissue temperature, although the differences are not big. It should be noted that in the two-temperature models, the blood temperature is lower than the temperature of the tissue (Fig. 3); therefore, a larger sub-domain of blood vessels corresponding to a higher value of porosity gives a lower tissue temperature [36, 37].
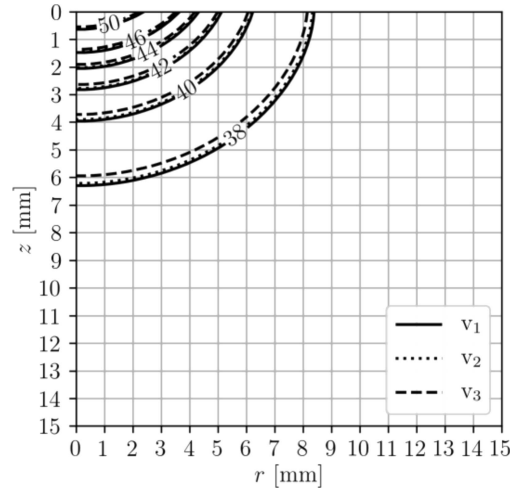

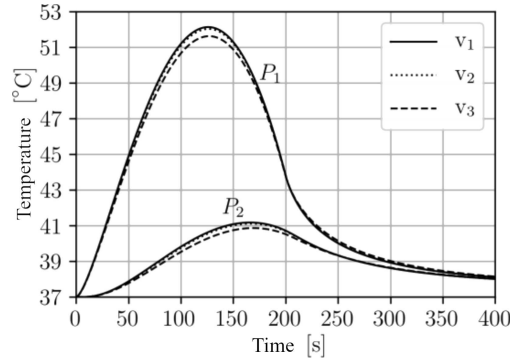**Fig. 1.** Tissue temperature distribution after 120 s for different variants of porosity.

Fig. 2. Tissue temperature history at the points P_1 (0.3; 0.3) [mm] and P_2 (1.5; 1.5) [mm] for different variants of porosity.
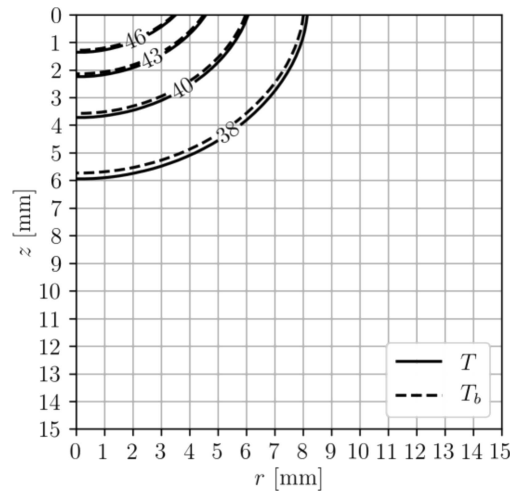
Fig. 3. Distribution of tissue and blood temperatures after 100 s for the third variant of porosity (v_3).

In Figs 4 and 5, the distributions of sensitivity functions $U_1 = \partial T/\partial q_0$ [K m^2/W] and $U_2 = \partial T/\partial t_e$ [K/s] are shown, while Figs 6 and 7 illustrate the courses of these functions at the two

selected points from the domain considered. Figure 4 presents the results after 120 seconds, which correspond to the maximum values of the sensitivity function U_1, as can be seen in Fig. 6. Figure 5 presents the results after 200 seconds, which correspond to the maximum values of the sensitivity function U_2, as can be seen in Fig. 7. The sensitivity functions have lower values for larger porosities.
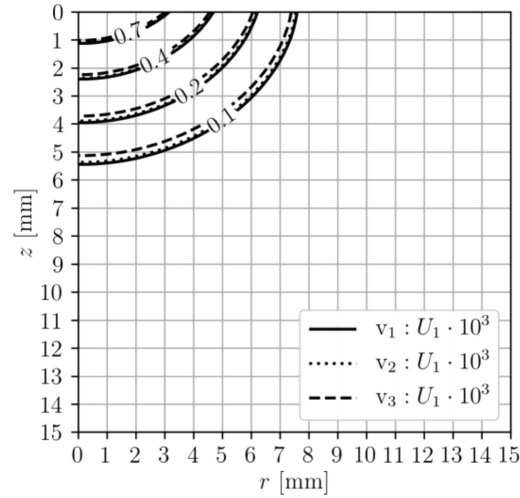
Fig. 4. Distribution of sensitivity function $U_1 = \partial T/\partial q_0$ [K m^2/W] after 120 s for different variants of porosity.
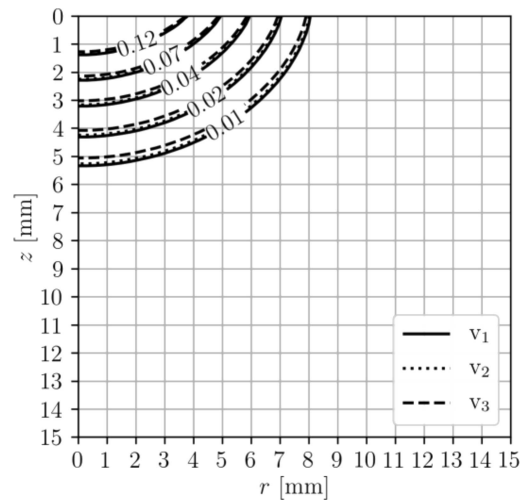
Fig. 5. Distribution of sensitivity function $U_2 = \partial T/\partial t_e$ [K/s] after 200 s for different variants of porosity.
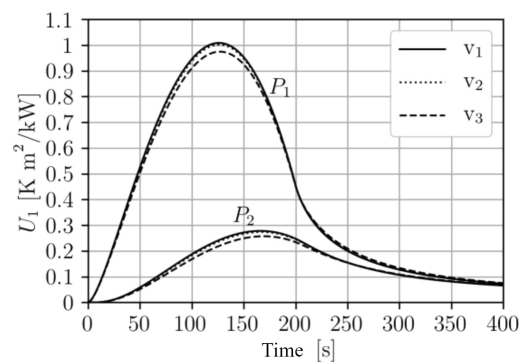
Fig. 6. Courses of sensitivity function $U_1 = \partial T/\partial q_0$ at the points P_1 (0.3; 0.3) [mm] and P_2 (1.5; 1.5) [mm] for different variants of porosity.
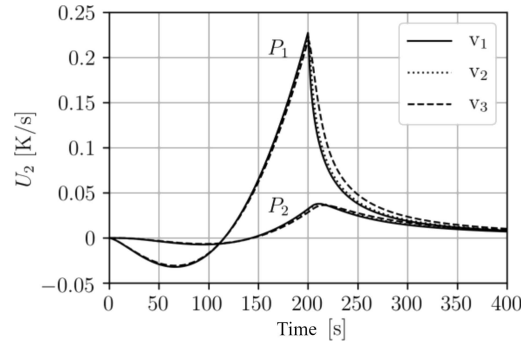
Fig. 7. Courses of sensitivity function $U_2 = \partial T / \partial t_e$ at the points P_1 (0.3; 0.3) [mm] and P_2 (1.5; 1.5) [mm] for different variants of porosity.

Figure 8 presents the distribution of Arrhenius integral after 400 seconds. The sub-domain of biological tissue in which the Arrhenius integral exceeds the value of 4.6 is destroyed. For a larger value of porosity, this sub-domain is slightly smaller.
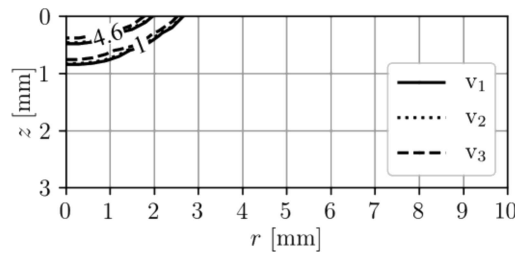

Fig. 8. Distribution of Arrhenius integral after 400 s for different variants of porosity (part of the cross-section).

Next, the inverse problem is solved. As mentioned earlier, based on the knowledge of the Arrhenius integral, the parameters q_0 and t_e in the Neumann boundary condition (9) are identified. It is assumed that the values of Arrhenius integral at fifty points uniformly distributed in the sub-domain $0 \leq r \leq 2.7$ mm and $0 \leq z \leq 2.7$ mm are known. These values are obtained from the direct problem solution. Below, the results for starting points $q_0 = 30$ kW/m^2, $t_e = 40$ s (variant sp$_1$), $q_0 = 12$ kW/m^2, $t_e = 400$ s (variant sp$_2$) and $q_0 = 37.5$ kW/m^2, $t_e = 500$ s (variant sp$_3$) are presented. For these values, the iteration process is convergent. Thus, in Figs 9 and 10, the values of parameters q_0 and t_e in subsequent iterations for the first variant of porosity are shown. As it can be seen, the number of iterations at which the real values are achieved depends on the starting point.

Figures 11–14 present the iteration process for different values of porosity and different starting points. For all variants, the iterative process is still convergent.
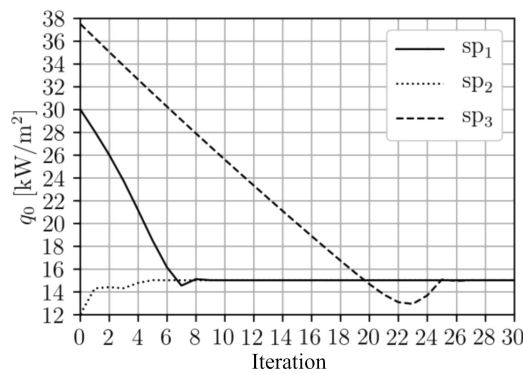

Fig. 9. Iteration process for the first variant of porosity and different starting points – parameter q_0.
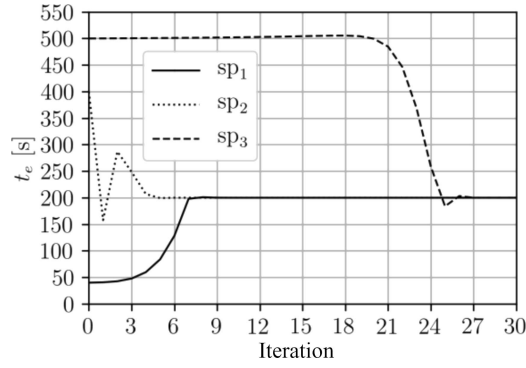
Fig. 10. Iteration process for the first variant of porosity and different starting points – parameter t_e.
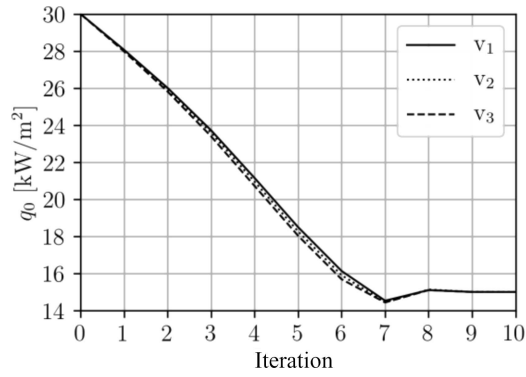

Fig. 11. Iteration process for starting point sp_1 and all variants of porosity – parameter q_0.
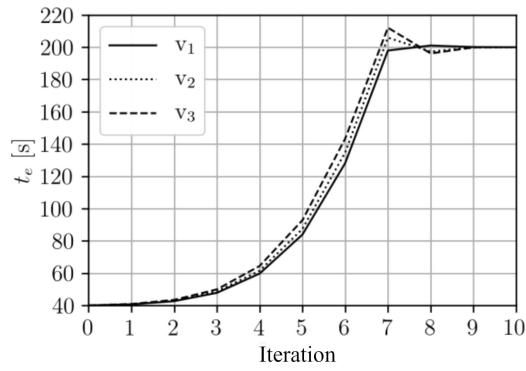

Fig. 12. Iteration process for starting point sp_1 and all variants of porosity – parameter t_e.
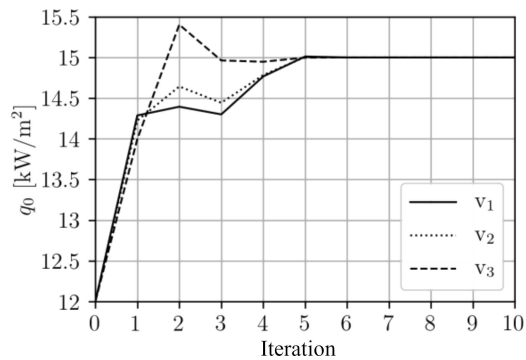

Fig. 13. Iteration process for starting point sp_2 and all variants of porosity – parameter q_0.
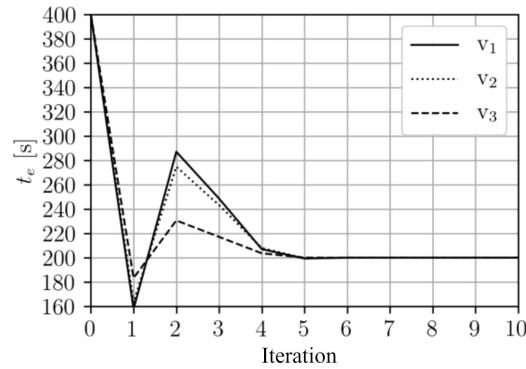
Fig. 14. Iteration process for starting point sp$_2$ and all variants of porosity – parameter t_e.

7. CONCLUSIONS

Thermal processes occurring in the axially symmetrical domain of heated tissue have been considered. This study aimed to estimate the boundary heat flux assuring the postulated destruction of the tissue target region. The direct problem has been described by the generalized dual-phase lag equation supplemented by appropriate boundary-initial conditions and has been solved using the implicit finite difference method. The inverse problem consisting in the identification of two parameters appearing in the Neumann boundary condition has been solved by means of the gradient method.

It should be noted that the iteration process was not always convergent. This paper presents the results only for those starting points, for which the iterative process was convergent. In future studies, it will be better to use a hybrid algorithm, which is a combination of an evolutionary algorithm and the gradient algorithm [38–43]. In the first stage, by using the evolutionary algorithm, it is possible to determine the starting point, and in the second stage, by using the gradient algorithm, determine the values of the identified parameters.

REFERENCES

[1] M.H. Niemz. *Laser-Tissue Interaction: Fundamentals and Applications*. Comptes Rendusdel' Académiedes Sciences-Series I-Mathematics, Springer-Verlag, Berlin, Heidelberg, Germany, 2002, doi: 10.1007/978-3-662-04717-0.

[2] S.A. Sapareto, W.C. Dewey. Thermal dose determination in cancer therapy. *International Journal of Radiation Oncology, Biology, Physics*, **10**(6): 787–800, 1984, doi: 10.1016/0360-3016(84)90379-1.

[3] M. Jasiński. Modelling of thermal damage in laser irradiated tissue. *Journal of Applied Mathematics and Computational Mechanics*, **14**(4): 67–78, 2015, doi: 10.17512/jamcm.2015.4.07.

[4] H.H. Pennes. Analysis of tissue and arterial blood temperatures in the resting human forearm. *Journal of Applied Physiology*, **85**(l): 93–122, 1984, doi: 10.1152/jappl.1948.1.2.93.

[5] M. Jamil, E.Y.K. Ng. Ranking of parameters in bioheat transfer using Taguchi analysis. *International Journal of Thermal Sciences*, **63**: 15–21, 2013, doi: 10.1016/j.ijthermalsci.2012.07.002.

[6] M. Ciesielski, B. Mochnacki. Application of the control volume method using the Voronoi polygons for numerical modeling of bio-heat transfer processes. *Journal of Theoretical And Applied Mechanics*, **52**(4): 927–935, 2014, doi: 10.15632/jtam-pl.52.4.927.

[7] B. Mochnacki, A. Piasecka-Belkhayat. Numerical modeling of skin tissue heating using the interval finite difference method. *MCB: Molecular & Cellular Biomechanics*, **10**(3): 233–244, 2013, doi: 10.3970/mcb.2013.010.233.

[8] E. Majchrzak, B. Mochnacki, M. Dziewoński, M. Jasiński. Numerical modelling of hyperthermia and hypothermia processes. *Advanced Materials Research*, **268–270**: 257–262, 2011, doi: 10.4028/www/scientific.net/AMR.268-270.257.

[9] E. Majchrzak, B. Mochnacki, M. Jasiński. Numerical modelling of bioheat transfer in multi-layer skin tissue domain subjected to a flash fire. *Computational Fluid and Solid Mechanics*, **1**(2): 1766–1770, 2003, doi: 10.4028/www.scientific.net/AMR.268-270.257.

[10] W. Kaminski. Hyperbolic heat conduction equation for materials with a nonhomogeneous inner structure. *Journal of Heat Transfer*, **112**(3): 555–560, 1990, doi: 10.1115/1.2910422.

[11] K. Mitra, S. Kumar, A. Vedevarz, M.K. Moallemi. Experimental evidence of hyperbolic heat conduction in processed meat. *Journal of Heat Transfer*, **117**(3): 568–573, 1995, doi: 10.1115/1.2822615.

[12] P.J. Antaki. New interpretation of non-Fourier heat conduction in processed meat. *Journal of Heat Transfer*, **127**(2): 189–193, 2005, doi: 10.1115/1.1844540.

[13] J. Zhou, J.K. Chen, Y. Zhang. Dual-phase lag effects on thermal damage to biological tissues caused by laser irradiation. *Computers in Biology and Medicine*, **39**(3): 286–293, 2009, doi: 10.1016/j.compbiomed.2009.01.002.

[14] J. Zhou, Y. Zhang, J.K. Chen. An axisymmetric dual-phase-lag bioheat model for laser heating of living tissues. *International Journal of Thermal Sciences*, **48**(8): 1477–1485, 2009, doi: 10.1016/j.ijthermalsci.2008.12.012.

[15] K.C. Liu, H.T. Chen. Investigation for the dual phase lag behavior of bio-heat transfer. *International Journal of Thermal Sciences*, **49**(7): 1138–1146, 2010, doi: 10.1016/j.ijthermalsci.2010.02.007.

[16] E. Majchrzak. Application of different variants of the BEM in numerical modeling of bioheat transfer processes. *MCB: Molecular & Cellular Biomechanics*, **10**(3): 201–232, 2013, doi: 10.3970/mcb.2013.010.201.

[17] E. Majchrzak, L. Turchan. The general boundary element method for 3D dual-phase lag model of bioheat transfer. *Engineering Analysis with Boundary Elements*, **50**: 76–82, 2015, doi: 10.1016/j.enganabound.2014.07.012.

[18] B. Mochnacki, E. Majchrzak. Numerical model of thermal interactions between cylindrical cryoprobe and biological tissue using the dual-phase lag equation. *International Journal of Heat and Mass Transfer*, **108**: 1–10, 2017, doi: 10.1016/j.ijheatmasstransfer.2016.11.103.

[19] Y. Zhang. Generalized dual-phase lag bioheat equations based on nonequilibrium heat transfer in living biological tissues. *International Journal of Heat and Mass Transfer*, **52**(21–22): 4829–4834, 2009, doi: 10.1016/j.ijheatmasstransfer.2009.06.007.

[20] N. Afrin, J. Zhou, Y. Zhang, D.Y. Tzou, J.K. Chen. Numerical simulation of thermal damage to living biological tissues induced by laser irradiation based on a generalized dual phase lag model. *Numerical Heat Transfer, Part A: Applications*, **61**(7): 483–501, 2012, doi: 10.1080/10407782.2012.667648.

[21] E. Majchrzak, Ł. Turchan, J. Dziatkiewicz. Modeling of skin tissue heating using the generalized dual-phase lag equation. *Archives of Mechanics*, **67**(6): 417–437, 2015.

[22] M. Jasiński, E. Majchrzak, L. Turchan. Numerical analysis of the interactions between laser and soft tissues using dual-phase lag model. *Applied Mathematical Modeling*, **40**(2): 750–762, 2016, doi: 10.1016/j.apm.2015.10.025.

[23] A.R.A. Khaled, K. Vafai. The role of porous media in modeling flow and heat transfer in biological tissues. *International Journal of Heat and Mass Transfer*, **46**(26): 4989–5003, 2003, doi: 10.1016/S0017-9310(03)00301-6.

[24] A. Nakayama, F. Kuwahara. A general bioheat transfer model based on the theory of porous media. *International Journal of Heat and Mass Transfer*, **51**(11–12): 3190–3199, 2008, doi: 10.1016/j.ijheatmasstransfer.2007.05.030.

[25] E. Majchrzak, Ł. Turchan. Numerical analysis of tissue heating using the bioheat transfer porous model. *Computer Assisted Methods in Engineering and Science*, **20**(2): 123–131, 2013.

[26] K. Kurpisz, A.J. Nowak. *Inverse Thermal Problems*. Computational Mechanics Publications, Southampton, Boston, 1995.

[27] M. Paruch. Identification of the cancer ablation parameters during RF hyperthermia using gradient, evolutionary and hybrid algorithms. *International Journal of Numerical Methods for Heat & Fluid Flow*, **27**(3): 674–697, 2017, doi: 10.1108/HFF-03-2016-0114.

[28] E. Majchrzak, B. Mochnacki. Sensitivity analysis and inverse problems in bio-heat transfer modelling. *Computer Assisted Mechanics and Engineering Sciences*, **13**: 85–108, 2006.

[29] M. Kleiber, H. Antúnez, T.D. Hien, P. Kowalczyk. *Parameter Sensitivity in Nonlinear Mechanics*. J. Willey & Sons, London, 1997.

[30] K. Dems, B. Rousselet. Sensitivity analysis for transient heat conduction in a solid body – Part I: External boundary modification. *Structural Optimization*, **17**(1): 36–45, 1999, doi: 10.1007/BF01197711.

[31] G. Kaluża, E. Majchrzak, Ł. Turchan. Sensitivity analysis of temperature field in the heated soft tissue with respect to the perturbations of porosity. *Applied Mathematical Modelling*, **49**: 498–513, 2017, doi: 10.1016/j.apm.2017.05.011.

[32] L. Turchan, E. Majchrzak. Identification of Neumann boundary condition assuring the destruction of target region of biological tissue. *Proceedings of the 9th International Conference on Computational Methods (ICCM 2018)*, August 6th–10th, Rome, Italy, **5**: 835–846, 2018.

[33] M. Paruch, Ł. Turchan. Mathematical modelling of the destruction degree of cancer under the influence of a RF hyperthermia. *AIP Conference Proceedings 1922*, Lublin, Poland, 2017, doi: 10.1063/1.5019064.

[34] C. Junmeng, H. Fang, Y. Weiming, Y. Fusheng. A new formula approximating the Arrhenius integral to perform the nonisothermal kinetics. *Chemical Engineering Journal*, **124**(1–3): 15–18, 2006, doi: 10.1016/j.cej.2006.08.003.

[35] A. Szasz, N. Szasz, O. Szasz. *Oncothermia: Principles and Practices*. Springer, Heidelberg, Germany, 2011, doi: 10.1007/978-90-481-9498-8.

[36] H.W. Huang, Z.P. Chen, R.B. Roemer. A counter current vascular network model of heat transfer in tissues. *Journal of Biomechanical Engineering*, **118**(1): 120–129, 1996, doi: 10.1115/1.2795937.

[37] S. Hassanpour, A. Saboonchi. Validation of local thermal equilibrium assumption in a vascular tissue during interstitial hyperthermia treatment. *Journal of Mechanics in Medicine and Biology*, **17**(5): 1750087 (26 pages), 2017, doi: 10.1142/S0219519417500877.

[38] T. Burczyński, W. Kuś, A. Długosz, P. Orantek. Optimization and defect identification using distributed evolutionary algorithms. *Engineering Applications of Artificial Intelligence*, **17**(4): 337–344, 2004, doi: 10.1016/j.engappai.2004.04.007.

[39] H. Li. An evolutionary algorithm for multi-criteria inverse optimal value problems using a bilevel optimization model. *Applied Soft Computing*, **23**: 308–318, 2014, doi: 10.1016/j.asoc.2014.06.044.

[40] Z. Michalewicz. *Genetic Algorithms + Data Structures = Evolution Programs.* Springer-Verlag, Berlin, 1996, doi: 10.1007/978-3-662-03315-9.

[41] M. Paruch. Identification of the degree of tumor destruction on the basis of the Arrhenius integral using the evolutionary algorithm. *International Journal of Thermal Sciences*, **130**: 507–517, 2018, doi: 10.1016/j.ijthermalsci.2018.05.015.

[42] E.G. Baquela, A.C. Olivera. A novel hybrid multi-objective metamodel-based evolutionary optimization algorithm. *Operations Research Perspectives*, **6**: 100098, 2019, doi: 10.1016/j.orp.2019.100098.

[43] F. Han, Q. Liu. A diversity-guided hybrid particle swarm optimization based on gradient search. *Neurocomputing*, **137**: 234–240, 2014, doi: 10.1016/j.neucom.2013.03.074.